Chapter 7 : High-frequency Plaque Characterization

High-frequency ultrasound imaging is useful for examining tissue structures and inhomogeneitites like calcifications -- it has the advantage of high resolution at the expense of low penetration. In this chapter new high frequency imaging techniques are explored for interrogation of the excised plaques which result from carotid endarterectomy procedures. First the materials and methods used to create these images are described. Note that many other details are found in Appendix A. Then, initial 3D parametric images of the excised plaques are presented.

7.1 Creation of parametric images of excised plaque

As mentioned in the Chapter 2, strain imaging holds promise because it is a direct measure of the local load the tissue is experiencing as opposed to approaches where measurements or assumptions of composition, geometry, and loading are used in a computational model or statistical classification to imply loading. An advantage to this approach is that errors from modeling simplifications and parameter measurements do not accumulate as significantly. The reference phantom method is analogous for ultrasonic tissue parameter characterization. Diffraction effects are measured empirically in a phantom environment similar to that expected *in situ* with minimal modeling or assumptions.

Approximately two weeks following the *in vivo* carotid ultrasound examination and TCD recording, patients undergo surgery for plaque excision. Endarterectomy specimens are retrieved

immediately following surgery for scanning and returned the same day to pathology for analysis and histology preparation. Samples are examined in a water bath and suspended between two catheter sheaths. A photograph of the experimental setup is shown in Fig. 7.1.

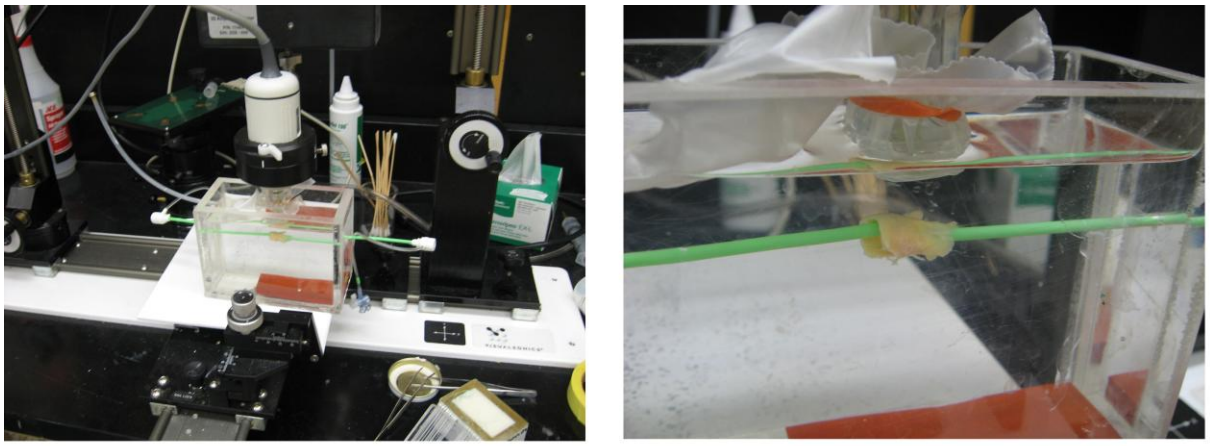

a) b)

Figure 7.1: High-frequency apparatus. The transducer is fixed to a 3D motion table and lowered into the water bath. A disposable transducer cover is covered with coupling gel and held to the transducer with a rubber band for safety reasons. The plaque is suspended between two catheter sheaths and the stepper motor moves the transducer parallel to the longitudinal direction of the plaque.

VisualSonics Vevo 770 is used for the high frequency ultrasound radiofrequency acquisition. The system for 3D collection and processing of RF data on the Vevo 770 is described in Appendix A.

The transducer selected is a RMV710B that has a center frequency of 25 MHz, which is on the lower end of the center frequency for available transducers. This transducer outputs frequencies up to 37.5 MHz, with an axial resolution of 70 μm, lateral resolution of 140 μm, focal length 15 mm, and a maximum field of view of 20.0 mm. The RMV710B is selected because the frequency is low enough to penetrate the plaque and the field of view is large enough

to encompass the entire sample.

RF acquisition was previously limited to single 2D frames, but we worked with VisualSonics engineers such that RF acquisitions can be collected in 3D with the optional high-precision stepper motor. Each acquisition consists of 250 beam lines separated by approximately 60 μm, 2128 samples (3.9 mm), and up to 250 frames separated by 200 μm to 100 μm depending on the length of the plaque specimen. Some longer plaques may require larger inter-frame spacing because of memory limitations, although the resolution in the elevational direction is nominally 140 μm for the RMV710B transducer.

For the lengths of the plaques scanned, which ranged from approximately 20 mm to 40 mm, this filled the system limits on acquisition. The collection of a single 3D data set covering an entire plaque takes approximately one to two hours. Resulting files are approximately 150 μm per volumetric slice. Three to five volumetric slices are required to encompass the majority of an excised plaque's volume. Some longer plaques may require larger inter-frame spacing because of memory limitations, although the resolution in the elevational direction is nominally 140 μm for the RMV710B transducer.

Integrated backscatter coefficient (IBSC) images are created with a reference phantom created by Dr. Ernest L. Madsen, PhD from UW-Madison. The reference phantom is made of the 5000E material characterized in Chapter 6. The reference phantom was scanned with the same transducer and system settings as utilized for scanning the plaque specimen. This includes the plastic covering over the transducer that prevents contamination of the transducer by plaque. Reference power spectra are obtained by averaging 30 lines per plane over 60 planes. Fourier spectra with 50% overlap are calculated using a Fast Fourier Transform with 128 Hamming windowed points (240 μm), and the bandwidth used ranged from 6.6 MHz to 29.6 MHz. The

BSC of the reference phantom is interpolated from the values measured with the reference reflector in Chapter 6. Attenuation in the plaque specimen was assumed to be the same as reference phantom, which is reasonable for arterial plaque specimens based on values reported in the literature [1, 2] The backscatter was calculated using the expression [3], below:

$$BSC_s(f) = \frac{BSC_r(f)S_s(f)}{S_r(f)}$$

Eqn. 7.1

Log compression and linear interpolation were applied to the displayed IBSC images. Identical dynamic ranges and color transform functions were used in all corresponding images.

7.2 B-Mode image creation

The received pulse-echo signal, that is RF data, is highly oscillatory. An envelope of the RF data reflects local scattering amplitude, and this is what comprises a B-Mode image.

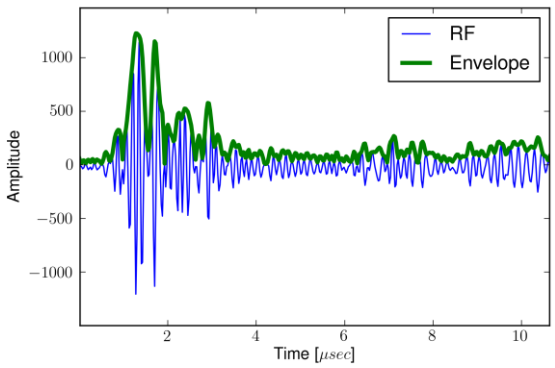

Figure 7.2: Sample RF signal and its corresponding envelope.

Calculation of the RF envelope is often performed with the analytic signal. The analytic

signal is used to decompose a signal into its local amplitude and phase [4, 5] [1]. The analytic signal, $f_A(x)$, of a real signal, $f(x)$, is defined to be

$$f_A(x) = f(x) - i\, f_H(x)$$

Eqn. 7.2

where $f_H(x)$ is the Hilbert Transform of $f(x)$ given by

$$f_H(x) = \frac{1}{\pi} \int_{-\infty}^{\infty} \frac{f(x')}{x' - x}\, dx'$$

Eqn. 7.3

The Hilbert Transform can be calculated without performing convolution by applying the following property in Fourier space,

$$F_H(\xi) = F(\xi) \cdot i\, \mathrm{sgn}(\xi)$$

Eqn. 7.4

As a result, the analytic signal's representation in Fourier space is

$$\begin{aligned} F_A(\xi) &= F(\xi) - i\, F_H(\xi) \\ &= F(\xi) - i\, F(\xi) \cdot i\, \mathrm{sgn}(\xi) \\ &= F(\xi) \cdot [1 + \mathrm{sgn}(\xi)] \end{aligned}$$

Eqn. 7.5

1 Local phase is a 1D concept, and the analytic signal is not defined for multi-dimensional signals. To split a multi-dimensional image into structural and energetic information, see the monogenic signal [4].

Even though it does not have ideal properties when applied to a discrete signal [6] an approach to calculate the analytic signal is then to calculate the Fourier Transform, multiply the first half by two, multiply the second half by zero, and take the inverse Fourier Transform.

For narrow band signals, the local phase, $\phi(x)$, and the local energy, *A(x)*, of *f(x)* can be interpreted as [4]

$$\begin{aligned} \phi(x) &= \tan^{-1}(f(x)/f_H(x)) \\ A(x) &= \sqrt{f^2(x) + f_H^2(x)} \end{aligned}$$

Eqn. 7.6

After the envelope, *A(x)*, is calculated, post-processing can be performed. The majority of an ultrasound image's content is speckle, random scattering caused by scatterers much smaller than the excitation wavelength, which follow a Rayleigh distribution [7]. Since the Rayleigh distribution is skewed to lower values and a very small proportion of the amplitudes having very large values, a logarithmic intensity transform is commonly applied to the envelope to improve image contrast.

7.3 3D high frequency plaque volumes

Gross photographic images taken prior to ultrasound scanning, B-mode images derived from the RF, and integrated backscatter coefficient (IBSC) images for two patients are shown in the following figures.

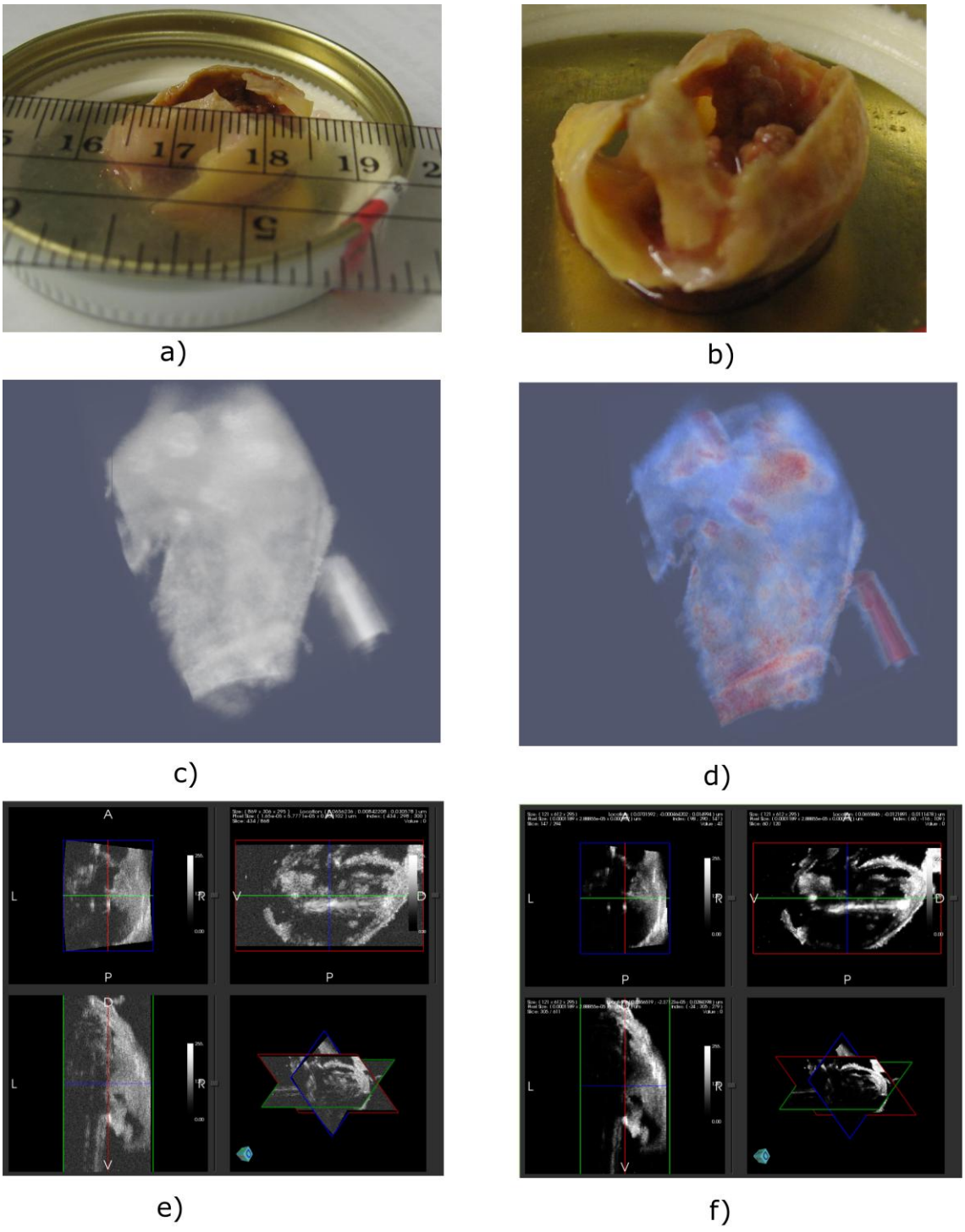

Figure 7.3: Images taken from the plaque excised from Subject 142. A large, diffuse hemorrhagic region shows decreased backscatter. a) Gross photographic image, b) close-up gross image, c) B-Mode volume rendering, d) integrated backscatter volume rendering, e) B-Mode tri-planar view, and f)

IBSC tri-planar view.

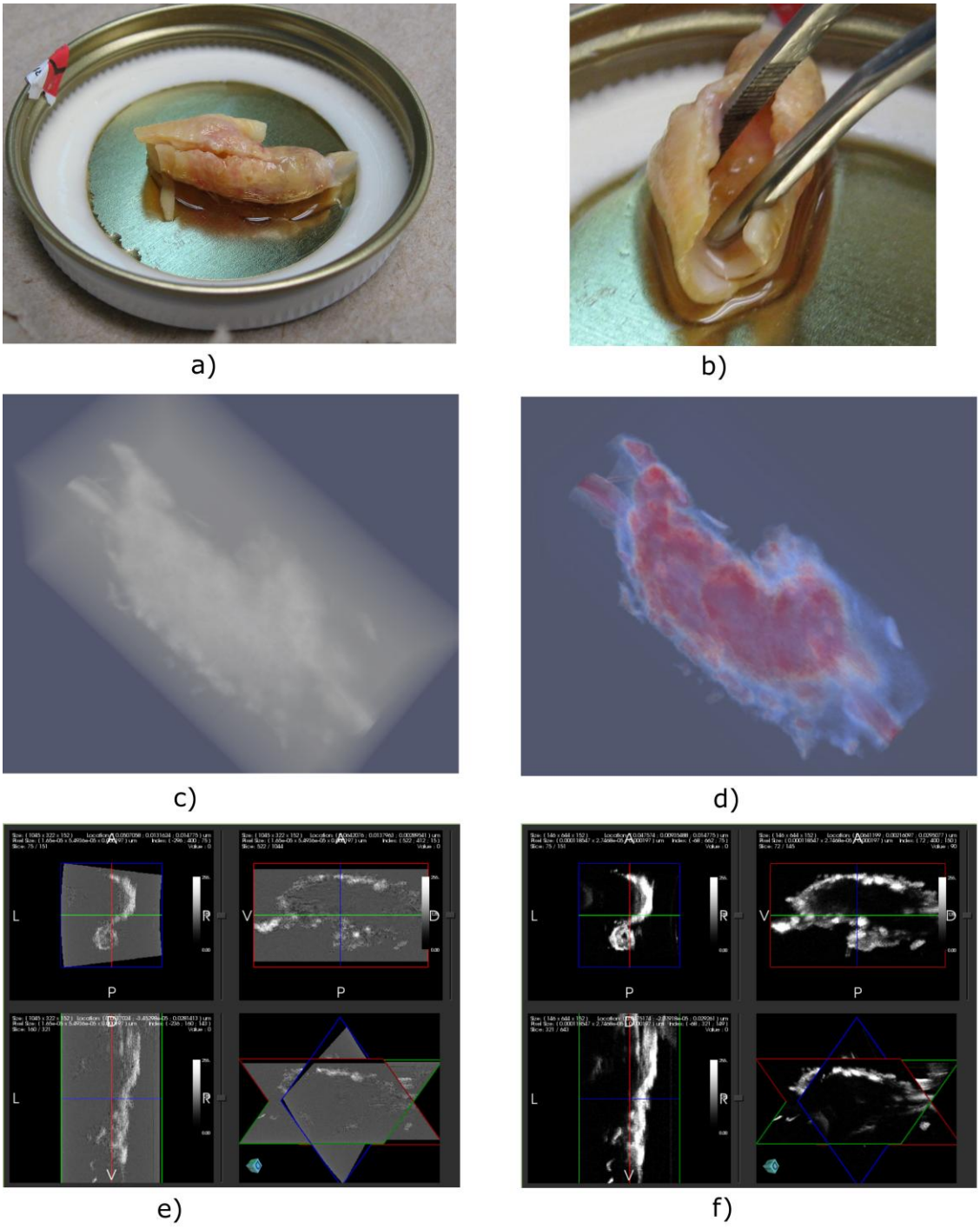

Figure 7.4: Images of the excised plaque from Subject 144. The gross photographs in a) and b) show a primarily fibrous plaque with some calcified areas. The ultrasound B-Mode, c) and e), and IBSC, d) and f), show the

presence of fibrous and calcified areas well. Segments from the catheter sheath are seen in the front and back of c) and d). To reduce saturation from numerous calcified areas, data was collected with -10 dB gain relative to Fig. 7.3a), which explains the larger impact of electronic noise in c).

Note the presence of the catheter used to suspend the plaques in these images. It is clearly visible as a high intensity cylinder. In Subject 142, as seen in Fig. 7.3, it is visible on the right and rear in the volume renderings. The catheter protrudes from the tips along the axis of the internal carotid artery (ICA) segment for Subject 144, shown in Fig. 7.4. It extends deeply into the bulb and ICA segment of Subject 154, as seen in Fig. 7.5. It reaches from the start of the bulb up into the bifurcation on one side and only slightly penetrates the ICA for Subject 158, in Fig. 7.6. In general, the IBSC images look 'cleaner' than the B-Mode images with similar spatial resolution. This can be attributed to the removal of speckle in the IBSC.

Subject 142 shows a possible high-risk plaque with an extensive hemorrhagic area that may have been the result of recent rupture events. There were strong indications of inflammation when this plaque was removed. The backscatter coefficient is consistently low throughout the hemorrhagic areas. This condition that is typically considered high risk and the high risk assessment is re-enforced by the fact that microembolic signals were detected with transcranial Doppler for Subject 142 (Table 8.1). The result for Subject 144 on the other hand, depicts a likely stable plaque with smooth, un-ulcerated walls and strong fibrous and calcified tissue throughout. Note the abundance of very high magnitude IBSC in Subject 144 because of calcifications. In a pathologist's independent assessment of the histopathological slides of the same specimens, Subject 142 was found to have approximately 5% calcified content, while Subject 144 was found to have 55% calcified content. This is consistent with the ultrasound results in Fig. 7.3 and Fig. 7.4.

The system receive gain was set 10 dB higher during the acquisition of plaques in Fig. 7.3

than that for Fig. 7.4. This reduced the amount of saturated signal due to the calcifications. However, this also increases the relative amplitude of electronic noise, which is most evident in the B-Mode volume rendering, shown in Fig. 7.4c). The purpose and benefits of the reference phantom methods are clearly illustrated in Fig. 7.4d), which is not duly affected by this change in the system settings. Since the electronic noise is equivalently elevated in the reference phantom signal, the change is nullified in terms of the output image. In comparison to the B-Mode image, the IBSC image is a more consistent representation of the object being profiled.

The tip of the flow divider, also known as the tuning fork, can be easily located in these images. This fiducial marker can be used to identify the corresponding region within *in vivo* data.

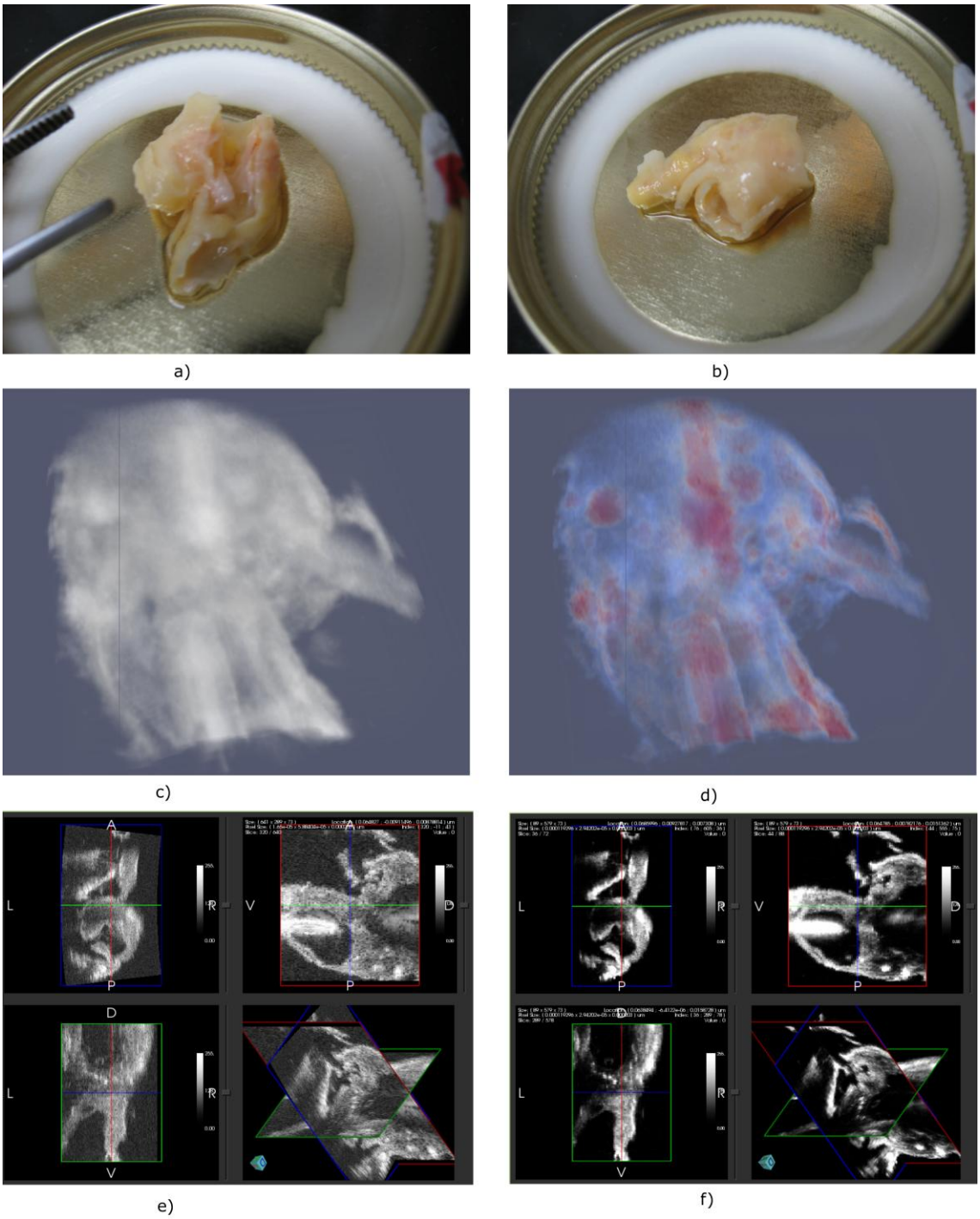

Figure 7.5: The excised plaque from Subject 154. *In vivo* strain characterization of this subject is shown in Figure 9.10. a) Gross photographic image, b) close-up gross image, c) B-Mode volume rendering, d) integrated backscatter volume rendering, e) B-Mode tri-planar view, and f) IBSC tri-planar view.

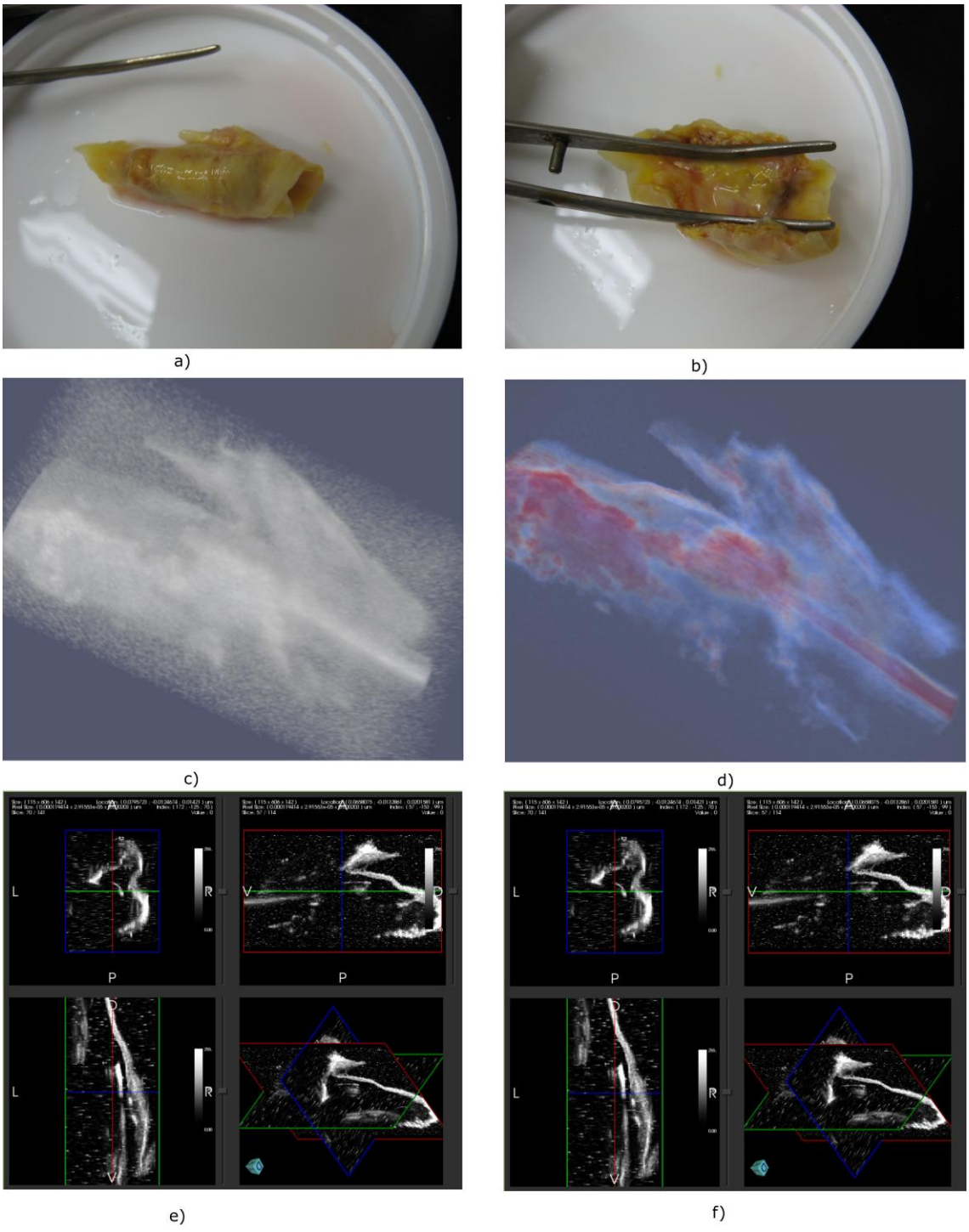

Figure 7.6: The excised plaque from Subject 158. *In vivo* strain characterization of this subject is shown in Figure 9.14. a) Gross photographic image, b) close-up gross image, c) B-Mode volume rendering, d) integrated backscatter volume rendering, e) B-Mode tri-planar view, and f) IBSC tri-

planar view.

Figure 7.5 and Fig. 7.6 show plaques attained from surgery that are used as strain case studies in Chapter 9. Subject 154, in Fig. 7.5 and Fig. 9.10, is used as an example of a plaque with a 'soft' hypoechoic presentation and that has high strain. Both the gross pathological appearance corroborates this assessment as does the 3D ultrasound characterization. The gross pathology shows a smooth, relatively homogeneous lipid and fibrous color. It is evident that the structure deforms under its own weight in comparison to the gross pathological image in Fig. 7.4. The IBSC image has low backscatter coefficients and is homogeneous with the exception of a few small pockets.

In contrast to Subject 154, a large acoustic shadow marks the B-Mode in Fig. 9.14. Very little strain is seen in the calcific region. However, other regions of the plaque do not exhibit the same shadowing, and some have very high strains. The gross pathology in Fig. 7.6a) and b) give a complex presentation with at least one region of hemorrhage/necrosis clearly visible in Fig. 7.6b). The ultrasound also shows a complex presentation with IBSC values consistent with calcific regions at the bifurcation and along one side of the ICA segment. It is possible that the focal, calcific region may explain the shadowing in Fig. 9.14 while the hemorrhagic regions could be the source of high strains. The noise present in the ultrasound images of Subject 158 is explained by a known malfunction of the transducer at that time.

In conclusion, 3D, high-frequency parametric ultrasound images may be a useful tool for plaque characterization. At a minimum, calcific areas can be identified. It was shown that the use of the reference phantom method improved the quality and content of the images. With a 3D volume, easy correlations are made between shapes in the gross pathology images and the ultrasound images. In the future, this data may be useful for registering histopathology slides

against regions within *in vitro* high-frequency ultrasound images, which in turn may be registered again external ultrasound to quantify the composition in the latter.

7.4 References

[1] P. R. Hoskins. Physical Properties of Tissues Relevant to Arterial Ultrasound Imaging and Blood Velocity Measurement. *Ultrasound in Medicine & Biology* 33, 1527--1539. 2007.

[2] G. R. Lockwood, L. K. Ryan, J. W. Hunt and F. S. Foster. Measurement of the ultrasonic properties of vascular tissues and blood from 35-65 MHz.. *Ultrasound Med Biol* 17, 653--666. 1991.

[3] W. Liu. In vivo ultrasound scatterer size imaging on liver tumors with a clinical scanner. 2007.

[4] M. Felsberg and G. Sommer. The monogenic signal. *IEEE Transactions on Signal Processing* 49, 3136--3144. 2001.

[5] J. Woo, B. Hong, C. Hu, K. K. Shung and C. Kuo. Non-Rigid Ultrasound Image Registration Based on Intensity and Local Phase Information. *Journal of Signal Processing Systems* 54, 33--43. 2008.

[6] R. N. Bracewell. *The Fourier Transform and Its Applications*. : McGraw-Hill. 2000.

[7] R. F. Wagner, S. W. Smith, J. M. Sandrik and H. Lopez. Statistics of Speckle in Ultrasound B-Scans. *IEEE Transactions on Sonics and Ultrasonics* 30, 156--163. 1983.